High performance TiN gate contact on AlGaN/GaN transistor using a mechanically strain induced P-doping

Ali Soltani, Michel Rousseau, Jean-Claude Gerbedoen, Maghnia Mattalah, P.L. Bonanno, A. Telia, Nour Eddine Bourzgui, Gilles Patriarche, A. Ougazzaden, A. Ben Moussa

Applied Physics Letters

High performance TiN gate contact on AlGaN/GaN transistor using a mechanically strain induced P-doping

Cite as: Appl. Phys. Lett. **104**, 233506 (2014); https://doi.org/10.1063/1.4882415
Submitted: 25 February 2014 • Accepted: 05 May 2014 • Published Online: 11 June 2014

A. Soltani, M. Rousseau, J.-C. Gerbedoen, et al.

High performance TiN gate contact on AlGaN/GaN transistor using a mechanically strain induced P-doping

A. Soltani,[1,a)] M. Rousseau,[1] J.-C. Gerbedoen,[1] M. Mattalah,[2] P. L. Bonanno,[3,4] A. Telia,[5] N. Bourzgui,[1] G. Patriarche,[6] A. Ougazzaden,[3,4] and A. BenMoussa[7]
[1]*Institut d'Electronique de Microélectronique et de Nanotechnologie, UMR-CNRS 8520, USTL, Avenue Poincaré, 59652 Villeneuve d'Ascq, France*
[2]*Laboratoire de Microélectronique, Université Djilali Liabès, 22000 Sidi Bel Abbès, Algeria*
[3]*School of Electrical and Computer Engineering, Georgia Institute of Technology, Atlanta, Georgia 30324-0250, USA*
[4]*UMI 2958 Georgia Tech-CNRS, Georgia Tech Lorraine, 2-3 Rue Marconi, 57070 Metz-Technopôle, France*
[5]*LMI, Electronic Department, Faculty of Engineering, Mentouri University of Constantine, Constantine, Algeria*
[6]*Laboratoire de Photonique et Nanostructures, CNRS UPR 20, Route de Nozay, 91460 Marcoussis, France*
[7]*Solar Terrestrial Center of Excellence, Royal Observatory of Belgium, Circular 3, B-1180 Brussels, Belgium*

(Received 25 February 2014; accepted 5 May 2014; published online 11 June 2014)

High performance titanium nitride sub-100 nm rectifying contact, deposited by sputtering on AlGaN/GaN high electron mobility transistors, shows a reverse leakage current as low as 38 pA/mm at $V_{GS} = -40$ V and a Schottky barrier height of 0.95 eV. Based on structural characterization and 3D simulations, it is found that the polarization gradient induced by the gate metallization forms a P-type pseudo-doping region under the gate between the tensile surface and the compressively strained bulk AlGaN barrier layer. The strain induced by the gate metallization can compensate for the piezoelectric component. As a result, the gate contact can operate at temperatures as high as 700 °C and can withstand a large reverse bias of up to −100 V, which is interesting for high-performance transistors dedicated to power applications. © *2014 AIP Publishing LLC*. [http://dx.doi.org/10.1063/1.4882415]

The gate control of High Electron Mobility Transistors (HEMTs) based on gallium nitride (GaN) semiconductors constitutes a crucial aspect of realizing devices presenting good linearity and high-frequency performances. This goal calls for a reliable rectifier contact to avoid gate leakage current reducing the breakdown voltage and consequently the microwave power performance. The process used to fabricate a rectifying contact constitutes currently a critical technological step, especially on GaN-based epitaxies grown at low temperature and with high aluminium (Al) content. In the past, extensive studies were carried out to fabricate different rectifying contacts on n-type AlGaN/GaN HEMTs in order to understand their formation and their conduction mechanisms.[1–3] Generally, the method consists of removing the native oxide of the AlGaN top surface layer by a chemical pre-treatment and then depositing refractory metals with high work functions such as molybdenum (Mo), nickel (Ni), or platinum (Pt).[4,5] A post-annealing is commonly performed to improve contact reliability.[6–8]

On the other hand, to form ohmic contacts on N-type III-Nitrides semiconductors, a titanium (Ti) layer is usually deposited by evaporation. After annealing at high temperature, a TiN layer is obtained on top of a complex structure based on metallic aggregates.

In our study, TiN rectifying contacts deposited by magnetron sputtering on $Al_{0.32}Ga_{0.68}N$/GaN HEMT structures are presented, showing a significant enhancement of the effective Schottky barrier height (Φ_B), a better charge control and a very low leakage current. It is found that the polarization gradient induced by the metallization strain in an AlGaN barrier forms a P-type pseudo-doping region. The strain induced by the gate metallization can compensate for the piezoelectric component under the gate. This component is usually largely responsible for the degradation of transistor performance.[9] A P-type pseudo-doping originating from the strain induced by TiN metallization constitutes a promising route towards a high-performance gate contact on GaN HEMTs.

The AlGaN/GaN epitaxial structures are grown by Picogiga International on a highly resistive (111)-oriented silicon substrate (20 kΩ cm) by Molecular Beam Epitaxy (MBE). A 0.54 μm-thick stress accommodation layer of AlN/GaN is deposited initially, followed by a 1.7 μm-thick buffer of $Al_{0.1}Ga_{0.9}N$, a 15 nm-thick channel of GaN, a 25 nm-thick barrier of $Al_{0.32}Ga_{0.68}N$, and a 1 nm-thick GaN cap layer. In a first step, the surface is ultrasonically cleaned and degreased by 1-min dip in HNO_3:H_2O (1:1), 1-min wet etch in HCl:H_2O (1:1), and then drying by nitrogen.

Ti/Al/Ni/Au (12/200/40/100 nm) evaporation is performed, followed by a rapid thermal annealing at 900 °C for 30 s in order to form ohmic contacts.[10] Components are isolated by He^+ ion implantation. As a result, an isolation current density of 850 nA/mm is measured at +150 V with a 8 μm space between the two contacts.

A rectifying contact is formed by Au/TiN sputtering and then lift-off using e-beam lithography for a 100 nm gate length (L_G). In order to maintain the material stoichiometry, we used a high purity (99.99%) TiN target. The lithography is performed under the following operating conditions: 100 W

a)Author to whom correspondence should be addressed. Electronic mail: ali.soltani@iemn.univ-lille1.fr.

radio frequency power at 13.56 MHz, 30 sccm argon (Ar) flow, and 220 V DC bias for an initial pressure of 3×10^{-7} millibars. The deposition rate is around 3.4 nm/min.

Different TiN film thicknesses from 2.5 nm to 150 nm and annealing temperatures from 300 °C to 900 °C have been tested. While the residual stress of an evaporated metal under high-vacuum conditions increases with the metal thickness, metals deposited by sputtering reach a maximum residual stress after only a few nm-thick deposition, decreasing thereafter with increased thickness.[11] In the case of TiN, a stress of 4.5 GPa is measured after a 7 nm-thick deposition.

Before the gate metallization, samples are deoxidized by HCl:H_2O (1:1) solution followed by *in situ* Ar^+ plasma etching. For $L_G = 100$ nm, the optimal Schottky contact performance (with 7 nm-thick TiN) is obtained after an annealing at 600 °C for 40 min in an N_2 atmosphere. Optical and scanning electron microscopy (SEM) measurements did not reveal any modifications of the contact surface morphology.

The patterns follow the Gate Transmission Line Method where the source-to-gate spacing (L_{GS}) is 1 μm. The ohmic contact resistance is 0.25 Ω mm associated with a specific contact resistance of 2×10^{-6} Ω·cm^2. From Hall measurements, we measured a sheet electron concentration of 8×10^{12} cm^{-2}, a carrier mobility of 1730 cm^2·V^{-1}·s^{-1}, and a sheet resistance of 460 Ω/sq. The transistor pinch-off voltage is −2.7 V.

Fig. 1 shows the $I_{GS} - V_{GS}$ characteristics of the Au/TiN gate contact before and after annealing at 600 °C. Before annealing, the I_{GS}–V_{GS} curve is interpreted through the thermionic emission theory and the field emission theory of Schottky barrier current transport. The transport behavior of a Schottky diode operating in the field emission regime ($V_G > 3kT/q$) is predicted by the following current-voltage equation:

$$I = I_S \times \exp[q(V_{GS} - R_S I_{GS})/\eta kT], \quad (1)$$

where I_S is the saturation current expressed by $I_S = SA^*T^2\exp(-q\phi_B/kT)$, q is the electron charge, T is the temperature in Kelvin, η is the ideality factor, A* is the effective Richardson constant, k is the Boltzmann constant,

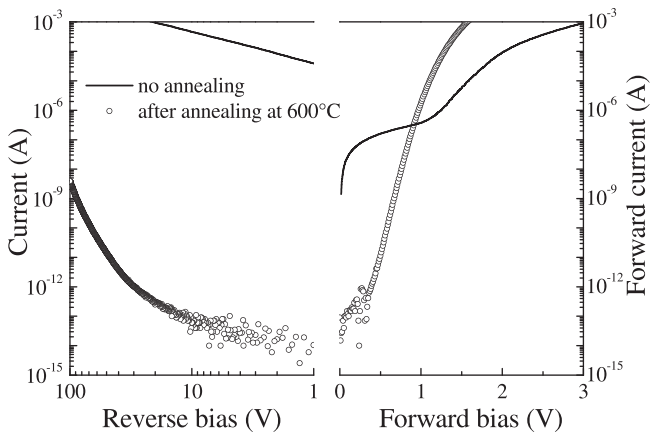

FIG. 1. I_{GS}–V_{GS} characteristics of Au/Tin Schottky contacts measured before and after annealing (gate width $W = 100\ \mu$m, $L_G = 100$ nm, $L_{GS} = 1\ \mu$m, $L_{GD} = 4\ \mu$m).

R_S is the series resistance, ϕ_B is the barrier height, and S is the contact area. A plot of $\log(I_{GS})$ versus V_{GS} is usually used to extract η where the slope of the linear region gives $q/\eta kT$. In this case, the gate contact presents a low ϕ_B of 0.4 eV associated with η of 6.8 and a leakage current of 14.7 mA/mm at $V_{GS} = -30$ V.

As shown in Fig. 1, after annealing at 600 °C, the reverse leakage current decreases by almost nine orders of magnitude. At −40 V, we measured a reverse leakage current of 38 pA/mm. Furthermore, under reverse bias at −100 V, the device exhibits a leakage current as low as 38.9 nA/mm. This rectifying contact shows a very stable behaviour and a good morphology up to 700 °C. The I_{GS}–V_{GS} forward characteristic exhibits a rectifier behavior with a significant enhancement of ϕ_B and is linear between 0.55 and 0.8 V. The series resistance R_S effect present in the diode model is taken into account and is evaluated to be 50 Ω at 300 K. In the following analysis, A* is calculated from the electron effective mass $m_e^* = 0.244m_0$ and is evaluated to be 33.36 A cm^{-2} K^{-2}. If the current transport is dictated by thermionic field emission theory, the relation between current and voltage can be expressed as

$$I = I_S\exp(V/E_0) \quad \text{with} \quad E_0 = E_{00}\coth\left(qE_{00}/kT\right) = \eta kT/q, \quad (2)$$

where E_{00} is the characteristic energy related to the transmission probability of carriers through the barrier given by the following equation:

$$E_{00} = h\left[\left(N_D/m_e^*\varepsilon_S\right)^{1/2}\right]/4\pi, \quad (3)$$

where h is the Planck constant, N_D is the donor concentration, ε_S is the semiconductor dielectric constant, and m_e^* is the electron effective mass. At 300 K, the ionized donor concentration N_D of GaN is determined from the $C_{GS}(V_{GS})$ measurement under reverse bias with $\varepsilon_S = 8.9$ and is evaluated to be 2.1×10^{15} cm^{-3}. The values of E_{00} and E_0 are around 0.57 meV and 37.2 meV, respectively. The Schottky barrier height ϕ_B and η are evaluated to be 0.95 eV and 1.41, respectively.

The Capacitance-Voltage (C_{GS}–V_{GS}) profiles measurement (not shown) is performed using a Precision LCR Meter with an internal bias supply (Hewlett Packard model 4284A) and a Semiconductor Parameter Analyzer (Agilent model 4155C). The measurement frequency range varies from 10 kHz to 1 MHz with an AC voltage amplitude of 10 mV. A delay time of 100 ms after setting the DC bias is used for all measurements. In the enhancement regime, this capacitance is constant whatever the frequency. Furthermore, no hysteresis is observed in the C_{GS}–V_{GS} curves, showing that the trapping effect is very low at the interface between TiN and AlGaN. This is in perfect agreement with the theoretical C_{GS}–V_{GS} calculation. This result reveals that there is no diffusion of TiN into the AlGaN barrier even after annealing as is confirmed by high resolution transmission electron microscopy (HRTEM), see in Fig. 2(b).

Fig. 2 shows nano-beam diffraction and HRTEM pictures of the Au/TiN/AlGaN interfaces of the Schottky contact obtained after thermal annealing at 600 °C where the

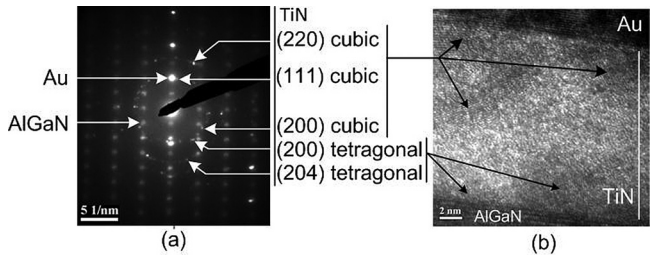

FIG. 2. (a) Nano-diffraction picture of the TiN metallization and (b) HRTEM picture of the same structure after thermal annealing at 600 °C.

different TiN phases can be observed. TiN metallization shows three phases along the thickness: a cubic structure on the Au side oriented (220) and (200), a tetragonal phase on the AlGaN side oriented (220) and (204), and a polycrystalline region between these two areas. Studies have shown a morphological transition of TiN films between 500 °C and 700 °C, which evolves according to the gate area, the gate length, and the TiN thickness. We did not observed AlO_x compounds at the TiN/AlGaN interface. In contrast to other commonly used Schottky metallization such as Au, Pt, or Ni which diffuses into the barrier layer during annealing, TiN metallization appears to be an excellent barrier even after high-temperature annealing.

As seen in Fig. 3, synchrotron radiation-based high-resolution X-ray diffraction (HRXRD) was carried out to measure strain relaxation in the AlGaN barrier layer at 10.4 keV energy at the 2-ID-D micro-diffraction beamline at the Advanced Photon Source at Argonne National Labs (USA). A zone plate setup allows us to focus the beam (with 180 arc sec divergence) to a quasi-circular illumination spot size of $r \approx 220$ nm. The device is mounted on an XYZ stage with 50 nm lateral resolution, and the location of our illumination spot was monitored via simultaneous measurement of Ga-K fluorescence intensities. Diffraction data are collected by a charge-coupled device (CCD) detector. Details of the description of the measuring station can be found in Ref. 12. Fig. 3 shows CCD captures of diffracted intensity from GaN (00.4) with the AlGaN barrier layer signal after annealing at 600 °C. It is clear that the c-plane compressive strain in the AlGaN barrier layer side source (Fig. 3(a)) and drain (Fig. 3(b)) are similar but under the gate, it decreases from −0.0138 to −0.0086 (Fig. 3(c)). In this last case, the AlGaN signal is closer to the GaN signal. We believe that the strain induced by the lattice mismatch at the AlGaN/GaN interface is partly compensated for by the surface strain resulting from the TiN metallization. This compensation is a function of the TiN thickness and of the annealing temperature.

In order to understand the physical behaviour of the TiN contact, we performed a modelling of the structure using the Tibercad® software.[13] The resulting strain in the AlGaN/GaN HEMT active area is calculated after applying an external surface force induced mechanically by the gate metallization. This allows us to simulate the strain induced by the lattice mismatch between the AlGaN barrier layer and GaN buffer layer. The calculation of the strain in lattice-mismatched heterostructures is based on the linear elasticity theory of solids, assuming pseudomorphic interfaces between different materials.[14]

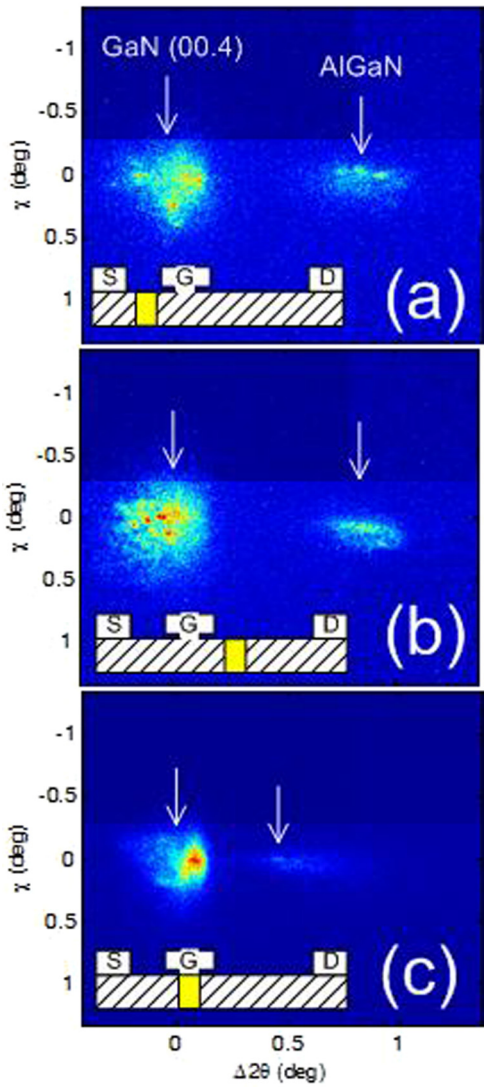

FIG. 3. Synchrotron-based XRD CCD captures showing clearly the (00.4) reflections of GaN (left-most signal in each CCD capture) and AlGaN. CCD diffraction intensity is shown in log scale and the scale is adjusted differently for each capture to better show the positions of the two signals. The horizontal axis of the captures roughly corresponds to the 2θ axis (q_z axis in reciprocal space), and the distance between the two signals along this axis represents increasing compressive strain in the AlGaN. The graphical representation of the HEMT structure indicates the localisation where each CCD capture was acquired.

For a small deformation u, the strain is

$$\varepsilon_{ik} = \frac{1}{2}\left(\frac{\partial u_l}{\partial x_k} + \frac{\partial u_k}{\partial x_i}\right). \tag{4}$$

The relationship between stress and strain is given by Hooke's law: $\sigma_{ik} = C_{iklm}\varepsilon_{lm}$.

The strain is found by minimizing the elastic energy

$$E = \frac{1}{2}\int_V \sigma_{ik}\varepsilon_{ik} dV. \tag{5}$$

As a result, we obtain the strain tensor in any point of the structure, the shape deformation, and the piezoelectric polarization, given by $P_i^{pz} = e_{ijk}\varepsilon_{jk}$. Self-consistent

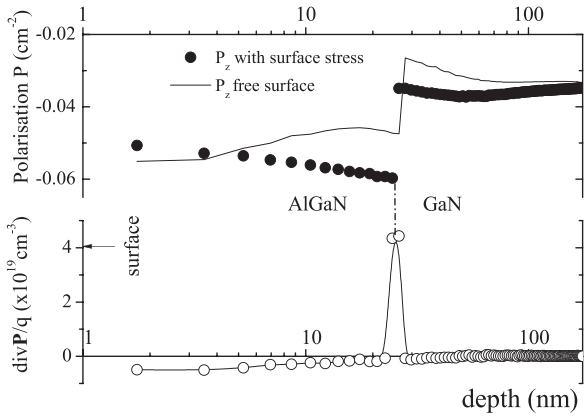

FIG. 4. Theoretical evolution of the polarization field in the AlGaN layer when applying a surface strain of 4.5 GPa and a surface potential of 0.4 eV. The inset shows the (div**P**)/q which show the nature of the pseudo-doping induced by strain gradient in the active area of the component.

electromechanical simulations can be carried out by including the piezoelectric effect. Semi-classical transport of electrons and holes is based on the drift-diffusion model.

Fig. 4 shows the theoretical evolution of the polarization in the AlGaN layer along the c-axis obtained by applying a surface strain of 4.5 GPa and a surface potential of 0.4 eV. The strain gradient in the AlGaN barrier layer induces a polarization gradient, which forms a pseudo p-doped AlGaN barrier layer. Div **P** is deduced and shows the nature of the pseudo-doping induced by the strain gradient and the net-piezoelectric charge at the AlGaN/GaN interface. The equivalent charge ρ_{eq} is related to the total polarization of the crystal P by

$$\rho_{eq} = N_A - N_D - \mathrm{div}\,\mathbf{P}. \quad (6)$$

This equation shows that a spatially changing polarization field creates a net bound charge in the crystal. This charge is referred to as a polarization charge and is fixed in space. This charge is positive at the AlGaN/interface and negative in the AlGaN barrier layer.

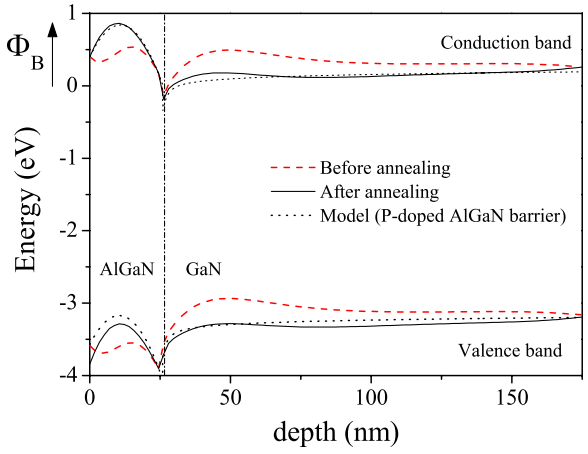

FIG. 5. Simulated band diagram of the heterostructure before and after the application of the external force obtained from Tibercad®. For comparison, Schrodinger-Poisson simulations are also shown.

Fig. 5 shows the simulated band diagram of AlGaN/GaN heterostructure obtained without (before annealing) and with (after annealing) an applied external force on the gate contact. The surface potential, which represents the barrier height of the TiN/HEMT ohmic contact, is fixed at 0.4 eV. The external force changes the electron barrier height from 0.4 eV to 0.87 eV, corresponding to a rectifier contact. As a comparison, a Schrodinger-Poisson simulation in the effective mass approximation is added with a P-AlGaN barrier layer at $3.65 \times 10^{18}\,\mathrm{cm}^{-3}$. A good agreement for the conduction-band is obtained, which confirms the p-doping of the AlGaN barrier layer.

The AlGaN/GaN HEMT behaviour was also investigated by means of DC pulse $I_{DS}(V_{DS})$ characteristics (not shown). Measurements were performed under different quiescent bias points V_{GS0} and V_{DS0}, to evaluate the lag effects. At $V_{DS0} = 5$ V, which corresponds to the worst condition, the current drops to only 3.8% ($V_{GS0} = -3$ V, $V_{DS0} = 0$ V) and 2.4% ($V_{GS0} = -3$ V, $V_{DS0} = 10$ V) due to gate and drain lag effects, respectively. Lag effects are very low, showing that good microwave power performance can be achieved. Furthermore, a good pinch-off behavior is observed, showing a good Schottky charge control in the device.

In conclusion, good performance TiN rectifying contacts are fabricated on a AlGaN/GaN HEMT. Our analysis shows that the strain mechanically induced by the gate metallisation removes a great part of the piezoelectric component under the gate and imposes a strain gradient in the AlGaN barrier layer, which forms a p-doping without doping impurities. The barrier height ϕ_B increases from 0.4 to 0.95 eV, and the reverse gate leakage current drastically drops down to 38 pA/mm at −40 V after a thermal annealing at 600 °C. The TiN Schottky contact shows a low reverse leakage current with low trapping phenomena under operating conditions which are necessary for high-performance transistors dedicated to power applications. Polarization-induced doping provides a solution to the problem of gate leakage current of AlGaN/GaN HEMTs without specific surface pretreatment.

The authors would like to acknowledge the French MOD (Delegation Generale pour l'Armement) for their financial support under Contract No. 06-137606/DGA/D4S/MRIS as well as Tibercad® developers for their useful support.

[1]Z. Lin, H. Kim, J. Lee, and W. Lu, Appl. Phys. Lett. **84**(9), 1585–1587 (2004).
[2]M. Kaneko and T. Hashizume, Phys. Status Solidi C **3**, 1758–1761 (2006).
[3]E. Ogawa, T. Hashizume, S. Nakazawa, T. Ueda, and T. Tanaka, Jpn. J. Appl. Phys., Part 2 **46**(24), L590–L592 (2007).
[4]T. Hashizume, J. Kotani, A. Basile, and M. Kaneko, Jpn. J. Appl. Phys., Part 2 **45**(4), L111–L113 (2006).
[5]A. Motayed, A. Sharma, K. A. Jones, M. A. Derenge, A. A. Iliadis, and S. Noor Mohammad, J. Appl. Phys. **96**(6), 3286–3295 (2004).
[6]H. Kim, M. L. Schuette, J. Lee, W. Lu, and J. C. Mabon, J. Electron. Mater. **36**(9), 1149–1155 (2007).
[7]C. Min Jeon and J. L. Lee, Appl. Phys. Lett. **82**(24), 4301–4303 (2003).
[8]H. Kim, J. Lee, L. Dongmin, and W. Lu, Appl. Phys. Lett. **86**, 143505 (2005).
[9]J. Joh, L. Xia, and J. A. Del Alamo, Tech. Dig. - Int. Electron Devices Meet. **2007**, 385–388.
[10]A. Soltani, A. BenMoussa, S. Touati, V. Hoel, J.-C. Dejaeger, J. Laureyns, Y. Cordier, C. Marhic, A. Djouadi, and C. Dua, Diamond Relat. Mater. **16**(2), 262–266 (2007).

[11]A. Stolz, A. Soltani, B. Abdallah, J. Charrier, D. Deresmes, P.-Y. Jouan, M. A. Djouadi, E. Dogheche, and J.-C. De Jaeger, Thin Solid Films **534**(1), 442–445 (2013).
[12]P. L. Bonanno, S. Gautier, A. A. Sirenko, A. Kazimirov, Z.-H. Cai, W. H. Goh, J. Martin, A. Martinez, T. Moudakir, N. Maloufi, M. B. Assouar, A. Ramdane, L. Le Gratiet, and A. Ougazzaden, Nucl. Instrum. Methods Phys. Res., Sect. B. **268**(3), 320–324 (2010).
[13]C. Majidi, Z. Chen, D. J. Srolovitz, and M. Haataja, J. Mech. Phys. Solids **58**, 73–85 (2010).
[14]M. Povolotskyi and A. Di Carlo, J. Appl. Phys. **100**(6), 063514 (2006).